Atom Indonesia

Journal homepage: http://atomindonesia.brin.go.id

Estimating $TPR_{20,10}$ Under Non-Reference Conditions Using a Geometric Sequence Approach

F. A. Rizaldi[1], S. Herwiningsih[1*], C. S. Widodo[1], F. K. Hentihu[2], A. K. Anto[2]

[1]*Physics Department, Faculty of Mathematics and Natural Sciences, Brawijaya University, Malang 65145, Indonesia*
[2]*Radiotherapy Department, Lavalette Hospital, Malang, 65111, Indonesia*

ARTICLE INFO

Article history:
Received 17 November 2024
Received in revised form 30 April 2025
Accepted 12 September 2025

Keywords:

$TPR_{20,10}$ under reference conditions
$TPR_{20,10}$ under non-reference conditions
Beam quality test of linear accelerator
Geometric sequence approach
X-ray megavoltage photon beam

ABSTRACT

An alternative approach to estimate the Tissue Phantom Ratio (TPR) at depths of 20 cm and 10 cm ($TPR_{20,10}$) under non-reference conditions is required to address situations where a 10 × 10 cm² field size is not achievable on a specific Linear Accelerator (LINAC) during a beam quality test. This study aims to estimate the $TPR_{20,10}$ under non-reference conditions using a geometric sequence approach, and to compare it with the $TPR_{20,10}$ under non-reference conditions estimated using the Sauer method, the Palmas method, a linear fit approach, as well as with the $TPR_{20,10}$ under reference conditions calculated using the TRS-398 protocol. The first step in this study was measuring the percentage depth dose (PDD), D_{20cm}, and D_{10cm} with field size variations from 4 × 4 cm² to 10 × 10 cm² for both 6 MV and 10 MV X-ray beams. The PDD were used to estimate the $TPR_{20,10}$ using a geometric sequence approach, the Sauer method, the Palmans method, and a linear fit approach, and to calculate the $TPR_{20,10}$ using the TRS-398 protocol. The D_{20cm} and D_{10cm} were also used to calculate the $TPR_{20,10}$ using the TRS-398 protocol. The $TPR_{20,10}$ for 6 MV and 10 MV X-ray beams estimated using the geometric sequence approach were 0.683 ± 0.004 and 0.742 ± 0.005, respectively. The level of precision that could be reached by the geometric sequence approach is potentially equivalent to the TRS-398 protocol, the Sauer method, the Palmans method, and the linear fit approach. The $TPR_{20,10}$ for 6 MV and 10 MV X-ray beams estimated using the geometric sequence method did not show a significant difference compared with the $TPR_{20,10}$ calculated using the TRS-398 protocol. However, the $TPR_{20,10}$ for 6 MV and 10 MV X-ray beams estimated using the geometric sequence approach showed a significant difference compared with those $TPR_{20,10}$ estimated using the Sauer method and the Palmans method.

INTRODUCTION

A Linear Accelerator (LINAC) is a teletherapy machine used to produce high-energy X-ray beams or high-energy electron beams [1]. One of the parameters tested in monthly Quality Control (QC) of a LINAC is the quality of the X-ray beam. The X-ray beam quality test is performed to ensure that the X-ray beam quality remains stable and does not deviate by more than 1% from the baseline [2]. X-ray beam quality represents the ability of an X-ray beam to penetrate a water phantom. It is determined based on the Tissue Phantom Ratio (TPR) at depths of 20 cm and 10 cm ($TPR_{20,10}$) or the Percentage Depth Dose (PDD) at a depth of 10 cm (PDD_{10}), measured in a water phantom under reference conditions [3].

*Corresponding author.
E-mail address: herwin@ub.ac.id
DOI:

The International Atomic Energy Agency (IAEA) in Technical Reports Series No. 398 (TRS-398) recommends two methods to estimate $TPR_{20,10}$ under reference conditions. The reference field size used to measure the absorbed dose in a water phantom is 10 × 10 cm². $TPR_{20,10}$ can be calculated from PDD [4], which is obtained by measuring the absorbed dose as a function of depth in a water phantom relative to its maximum dose [5]. $TPR_{20,10}$ can also be calculated from the absorbed dose in a water phantom at depths of 20 cm and 10 cm [4]. However, in situations where a 10 × 10 cm² field size is not achievable on a specific LINAC, these methods cannot be used to calculate $TPR_{20,10}$ under reference conditions [6-8].

There are two alternative methods recommended by IAEA in the Technical Reports Series No. 483 (TRS-483) to estimate $TPR_{20,10}$ under non-reference conditions, namely the Sauer method and the Palmans method [8]. Nevertheless, both the

Sauer method and the Palmans method are less suitable for a LINAC which has baseline data of $TPR_{20,10}$ that differ from those reported in the British Journal of Radiology Supplement 25 (BJR Sup. 25) [6,7,9]. Previous research has shown that the linear fit approach can also be used to estimate the $TPR_{20,10}$ under non-reference condition. This approach showed good agreement with both the Sauer method and Palmans method [9].

In this study, the $TPR_{20,10}$ under non-reference conditions were estimated using the geometric sequence approach. Furthermore, the $TPR_{20,10}$ estimated using the geometric sequence approach were compared with the $TPR_{20,10}$ estimated using the Sauer method, the Palmans method, and the linear fit approach, as well as with the $TPR_{20,10}$ calculated using the TRS-398 protocol.

THEORY AND CALCULATION

Tissue Phantom Ratio (TPR)

TPR is an indicator of beam quality that represents the exponential attenuation of an X-ray beam in a water phantom [10]. The higher the beam quality, the deeper the penetration ability of an X-ray beam in a water phantom. $TPR_{20,10}$ has a characteristic value for each X-ray beam energy. Therefore, its value differs for each X-ray beam energy used [3].

Calculation of $TPR_{20,10}$ using the TRS-398 protocol

First, $TPR_{20,10}$ was calculated from the PDD at depths of 20 cm and 10 cm in a water phantom using Eq. (1) [11,12]:

$$TPR_{20,10} = 1{,}2661\frac{PDD_{20}}{PDD_{10}} - 0{,}0595 \quad (1)$$

where $TPR_{20,10}$ refers to the TPR at depths of 20 cm and 10 cm under reference conditions, while PDD_{20} and PDD_{10} refer to the PDD at depths of 20 cm and 10 cm, respectively, measured under reference conditions [11,12].

Second, $TPR_{20,10}$ was calculated from the absorbed dose at depths of 20 cm and 10 cm in a water phantom using Eq. (2) [4]:

$$TPR_{20,10} = \frac{D_{20cm}}{D_{10cm}} \quad (2)$$

where D_{20cm} and D_{10cm} refer to the absorbed doses at depths of 20 cm and 10 cm, measured under reference conditions [4].

Estimation of $TPR_{20,10}$ using the sauer method

The Sauer method is a method proposed by Otto Andreas Sauer used to estimate the $TPR_{20,10}$ under non-reference conditions. The equation of the Sauer Method is expressed in Eq. (3) [7]:

$$Q = \frac{\left(TPR_{20,10}(s) - \left(b_1 + A_1\left(1 - e^{-\frac{S}{t}}\right)\right)\right)}{\left(b_2 + A_2\left(1 - e^{-\frac{S}{t}}\right)\right)} \quad (3)$$

where Q refers to the $TPR_{20,10}$ under non-reference conditions, $TPR_{20,10}$ (s) refers to the measured $TPR_{20,10}$ with an arbitrary field size, S is an arbitrary field size, and the variables b_1, b_2, t, A_1, A_2 are constants [7].

Estimation of $TPR_{20,10}$ using the palmans method

The Palmans method is a method proposed by Hugo Palmans used to estimate the $TPR_{20,10}$ under non-reference conditions. The equation of the Palmans Method is expressed in Eq. (4) [6] :

$$TPR_{20,10} = \frac{TPR_{20,10}(s) + d_1(10 - S)}{1 + d_2(10 - S)} \quad (4)$$

where $TPR_{20,10}$ refers to the $TPR_{20,10}$ under non-reference conditions, $TPR_{20,10}$ (s) refers to is the measured $TPR_{20,10}$ with an arbitrary field size, S is an arbitrary field size, while the variables d_1 and d_2 are constants [6].

Estimation of $TPR_{20,10}$ using a linear fit approach

A linear fit approach is used to estimate the $TPR_{20,10}$ under non-reference conditions using linear regression. The equation of the linear regression is obtained by plotting a linear regression graph of field sizes versus $TPR_{20,10}$ under non-reference conditions [9].

Estimation of $TPR_{20,10}$ using a geometric sequence approach

The $TPR_{20,10}$ with field size variations from 4 × 4 cm² to 10 × 10 cm² reported in BJR Sup.25 show a pattern similar to the geometric sequence [9]. Therefore, the geometric sequence approach should be able to estimate the $TPR_{20,10}$ under non-reference conditions [13,14]. Accordingly, this approach is explored in this study.

METHODS

Measurement of PDD

The PDD measurements were performed according to the TRS-483 protocol [8]. The measurement instruments and LINAC parameters are tabulated in Tables 1 and 2. Figure 1 shows the measurement setup of PDD.

Table 1. Measurement instruments for measuring PDD, D_{20cm}, and D_{10cm}.

Measurement instruments	
Water phantom	MP1 phantom tanks (PTW, Freiburg, Germany)
Ionization chamber	Semiflex chamber type 31010 (PTW, Freiburg, Germany)
Electrometer	Tandem dual channel electrometers (PTW, Freiburg, Germany)
LINAC	LINAC Elekta Synergy Platform (Elekta, Stockholm, Sweden)

Table 2. LINAC parameters for measuring PDD, D_{20cm}, and D_{10cm}.

LINAC parameters	Values
X-ray beam energy	6 MV and 10 MV
Field size variations for measuring PDD	4 × 4 cm², 5 × 5 cm², 6 × 6 cm², 7 × 7 cm², 8 × 8 cm², 9 × 9 cm², and 10 × 10 cm²
Field size for measuring D_{20cm} and D_{10cm}	10 × 10 cm²
Source-to-surface distance (SSD) for measuring PDD	100 cm
Source-to-chamber distance (SCD) for measuring D_{20cm} and D_{10cm}	100 cm

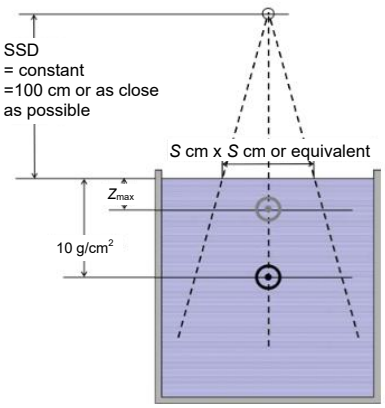

Fig. 1. Measurement setup of PDD_{10} (S×S cm²) [8].

Calculation of $TPR_{20,10}$ from PDD using the TRS-398 protocol

The PDD_{20} and PDD_{10} obtained from the PDD measurement under reference conditions were used to calculate the $TPR_{20,10}$ using Eq. (1) [4]. The calculated $TPR_{20,10}$ were averaged with the $TPR_{20,10}$ from the LINAC's monthly QC conducted from January 2022 to February 2023. This was possible because the $TPR_{20,10}$ from the LINAC's monthly QC were also calculated from the PDD using the TRS-398 protocol [2].

Estimation of $TPR_{20,10}$ using the geometric sequence approach

The $TPR_{20,10}$ (s) was calculated using the PDD with field size variations from 4×4 cm² to 9×9 cm² using Eq. (1). All $TPR_{20,10}$ (s) were modeled as the U_n term of the geometric sequence based on the field size variations as shown in Table 3.

Table 3. Modeling of $TPR_{20,10}$ as the U_n term.

$TPR_{20,10}$ (S × S cm²)	U_n
$TPR_{20,10}$ (10 ×10 cm²)	U_1
$TPR_{20,10}$ (9 × 9 cm²)	U_2
$TPR_{20,10}$ (8 × 8 cm²)	U_3
$TPR_{20,10}$ (7 × 7 cm²)	U_4
$TPR_{20,10}$ (6 × 6 cm²)	U_5
$TPR_{20,10}$ (5 × 5 cm²)	U_6
$TPR_{20,10}$ (4 × 4 cm²)	U_7

The first term (U_1) is started at 10 × 10 cm² to ensure the ratio (r) is within the range $-1 < r < 1$. As a result, the term of the geometric sequence will always be a finite number [13]. The ratio between consecutive terms was calculated to estimate the U_1 using the geometric sequence from U_3 to U_7, and the estimated values of U_1 were averaged.

Estimation of $TPR_{20,10}$ using the sauer method and the palmans method

The $TPR_{20,10}$ (s) were used to estimate the $TPR_{20,10}$ using Eq. (3) for the Sauer method and Eq. (4) for the Palmans method [8]. Then, the estimated $TPR_{20,10}$ values obtained using the Sauer method and the Palmans method were averaged separately.

Estimation of $TPR_{20,10}$ using the linear fit approach

The $TPR_{20,10}$ (s) and their field sizes were plotted using SPSS software version 27 (IBM Corporation, Armonk, United States). The x-axis represented the field sizes and the y-axis represented the $TPR_{20,10}$ (s). The linear regression equation was used to estimate the $TPR_{20,10}$ by substituting $x = 10$ into the equation [9].

Calculation of $TPR_{20,10}$ from absorbed dose using the trs-398 protocol

The D_{20cm} and D_{10cm} measurements were performed according to the TRS-398 protocol. Measurements of D_{20cm} and D_{10cm} were performed in three repetitions [4]. The measurement instruments and LINAC parameters are tabulated in Tables 1 and 2. Figure 2 shows the measurement setup for D_{20cm} and D_{10cm}.

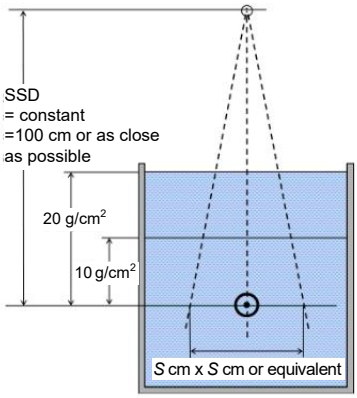

Fig. 2. Measurement setup of $TPR_{20,10}$ (S×S cm²) [8].

The D_{20cm} and D_{10cm} values under reference conditions were used to calculate the $TPR_{20,10}$ using Eq. (2), and the calculated values of $TPR_{20,10}$ were averaged [4].

Calculation of relative differences

The relative difference between the estimated $TPR_{20,10}$ and the $TPR_{20,10}$ baseline data was calculated using Eq. (5) [4].

$$RD = \left| \frac{\left(TPR_{20,10} - TPR_{20,10_{ref}}\right)}{TPR_{20,10_{ref}}} \right| \times 100\% \qquad (5)$$

where RD refers to the relative difference (%), $TPR_{20,10}$ refers to the estimated $TPR_{20,10}$, and $TPR_{20,10}$ Ref refers to the $TPR_{20,10}$ baseline data. Due to the unavailability of the $TPR_{20,10}$ baseline data in Lavalette Hospital, the PDD baseline data were converted to $TPR_{20,10}$ using Eq. (1), and these value were used as the $TPR_{20,10}$ Ref. [4].

Comparison of $TPR_{20,10}$ estimation result

The $TPR_{20,10}$ estimated using the geometric sequence approach was compared with the $TPR_{20,10}$ estimated using the two methods recommended by the IAEA in TRS-483 and the linear fit approach. In addition, it was compared with the $TPR_{20,10}$ calculated using the two methods recommended by the IAEA in TRS-398. Furthermore, mean comparisons were performed using the paired T-test and the Durbin-Watson test in SPSS software version 27 [15,16].

RESULTS AND DISCUSSION

Estimation of $TPR_{20,10}$ using the geometric sequence approach

The $TPR_{20,10}$ estimated using the geometric sequence approach is tabulated in Table 4.

Table 4. Estimation results of the $TPR_{20,10}$ using the geometric sequence approach.

X-ray energy	Field size	$TPR_{20,10}$	Mean ± SD[a]
6 MV	4×4 cm²	0.677	0.683 ± 0.004
	5×5 cm²	0.687	
	6×6 cm²	0.687	
	7×7 cm²	0.680	
	8×8 cm²	0.682	
10 MV	4×4 cm²	0.748	0.742 ± 0.005
	5×5 cm²	0.743	
	6×6 cm²	0.743	
	7×7 cm²	0.736	
	8×8 cm²	0.738	

[a] Standard deviation (SD)

Table 4 shows that the $TPR_{20,10}$ for the 10 MV X-ray beam was greater than the $TPR_{20,10}$ for the 6 MV X-ray beam. This occurs because the higher the X-ray energy used, the deeper the X-ray penetration in the water phantom [3].

The X-ray energy depends on the accelerator tube used. This is because a higher voltage in the accelerator tube results in a greater electric potential. As the electric potential increases, the potential difference inside the accelerator tube also increases. Consequetly, the electrons in the accelerator tube are accelerated, converting their potential energy into kinetic energy [17,18].

Inside the accelerator tube, the speed of the electron beam is further increased by electromagnetic waves, resulting in a higher kinetic energy of the electron beam. When the electron beam interacts with the target, its kinetic energy is converted into heat and X-ray beam [19].

Comparison of $TPR_{20,10}$ estimated using the geometric sequence approach with $TPR_{20,10}$ calculated using the TRS-398 protocol.

Table 5 shows the $TPR_{20,10}$ estimated using the geometric sequence approach and the $TPR_{20,10}$ calculated using the TRS-398 protocol.

In Table 5, the $TPR_{20,10}$ estimated using the geometric sequence approach did not significantly differ from the $TPR_{20,10}$ calculated using the TRS-398 protocol. This shows that the geometric sequence approach is in good agreement with the TRS-398 protocol [20]. Furthermore, the standard deviation of the $TPR_{20,10}$ estimated using the geometric sequence approach was slightly different from the standard deviation of the $TPR_{20,10}$ calculated using the TRS-398 protocol. This shows that the precision level of the geometric sequence approach was equivalent to that of the TRS-398 protocol [20]. Table 6 shows the P-values of the $TPR_{20,10}$ estimated using the geometric sequence approach paired with the $TPR_{20,10}$ calculated using the TRS-398 protocol.

Table 5. $TPR_{20,10}$ estimated using the geometric sequence approach and $TPR_{20,10}$ calculated using the TRS-398 protocol.

X-ray energy	Mean ± standard deviation		
	Geometric sequence approach	TRS-398 protocols	
		Calculated from PDD	Calculated from D_{20cm} and D_{10cm}
6 MV	0.683 ± 0.004	0.681 ± 0.001	0.680 ± 0.001
10 MV	0.742 ± 0.005	0.735 ± 0.001	0.736 ± 0.001

Table 6. Paired T-test of the $TPR_{20,10}$ estimated using the geometric sequence approach with the $TPR_{20,10}$ calculated using the TRS-398 protocol.

X-ray energy	Pair number	Paired method		P-value
6 MV	Pair 1	GS[a]	CP[b]	0.548
	Pair 2		CD[c]	0.405
10 MV	Pair 3	GS[a]	CP[b]	0.058
	Pair 4		CD[c]	0.037

[a] Geometric sequence approach (GS)
[b] Calculation from PDD data based on TRS-398 protocol, (CP)
[c] Calculation from D_{20cm} and D_{10cm} based on TRS-398 protocol (CD)

In Table 6, the P-values for Pairs 1, 2, and 3 were greater than 0.05. This shows that the $TPR_{20,10}$ estimated using the geometric sequence approach and the $TPR_{20,10}$ calculated using the TRS-398 protocol were not significantly different. However, the P-value for Pair 4 was less than 0.05. This shows that the $TPR_{20,10}$ estimated using the geometric sequence approach and the $TPR_{20,10}$ calculated from the D_{20cm} and D_{10cm} were significantly different [21].

Comparison of estimated $TPR_{20,10}$

Table 7 shows the $TPR_{20,10}$ estimated using the geometric sequence approach, the Sauer method, the Palmans method, and the linear fit approach.

In Table 7, the standard deviation of the $TPR_{20,10}$ calculated using the geometric sequence approach was slightly different from the standard deviation of the $TPR_{20,10}$ calculated using the Sauer method, the Palmans method, and the linear fit approach. This indicates that the geometric sequence approach has a precision level equivalent to that of the Sauer method, the Palmans method, and the linear fit approach [20]. Table 8 shows the P-values of the $TPR_{20,10}$ estimated using the geometric sequence method paired with the $TPR_{20,10}$ estimated using the Sauer method, the Palmans method, and the linear fit approach.

Table 7. $TPR_{20,10}$ estimated using the geometric sequence and linear fit approaches, the Sauer method, and the Palmans method.

Method	Mean ± Standard deviation	
	6 MV	10 MV
Geometric sequence approach	0.683 ± 0.004	0.742 ± 0.005
Sauer method	0.675 ± 0.002	0.732 ± 0.003
Palmans method	0.675 ± 0.003	0.731 ± 0.001
Linear fit approach	0.682 ± 0.001	0.741 ± 0.001

Table 8. Paired T-test of the $TPR_{20,10}$ estimated using the geometric sequence approach with the $TPR_{20,10}$ estimated using the Sauer methood, the Palmans method, and the linear fit approach.

X-ray energy	Pair Number	Paired Method		P-value
6 MV	Pair 1	GS[a]	SA[b]	0.030
	Pair 2		PA[c]	0.046
	Pair 3		LF[d]	0.461
10 MV	Pair 4	GS[a]	SA[b]	0.045
	Pair 5		PA[c]	0.048
	Pair 6		LF[d]	0.857

[a] Geometric sequence approach (GS)
[b] Sauer method (SA)
[c] Palmans method (PA)
[d] Linear fit approach (LF)

Table 9. Relative difference between the $TPR_{20,10}$ estimated using the geometric sequence approach, the TRS-398 protocol, the TRS-483 protocol, and the linear fit approach.

X-ray energy	Relative difference to $TPR_{20,10}$ calculated from PDD data			
	Geometric sequence	Sauer method	Palmans method	Linear fit method
6 MV	0.29%	0.88%	0.88%	0.15%
10 MV	0.95%	0.41%	0.54%	0.82%
X-ray energy	**Relative difference to $TPR_{20,10}$ calculated from D_{20cm} and D_{10cm}**			
	Geometric sequence	Sauer method	Palmans method	Linear fit method
6 MV	0.44%	0.74%	0.74%	0.29%
10 MV	0.82%	0.54%	0.68%	0.68%

In Table 8, the P-values for Pairs 1, 2, 4, and 5 were less than 0.05. This shows that the $TPR_{20,10}$ estimated using the geometric sequence approach and the $TPR_{20,10}$ estimated using the Sauer method and the Palmans method were significantly different. However, the P-values for Pairs 3 and 6 were greater than 0.05. This shows that the $TPR_{20,10}$ estimated using the geometric sequence approach and the $TPR_{20,10}$ estimated using the linear fit approach were not significantly different [21]. Table 9 shows a comparison of the relative difference between the $TPR_{20,10}$ estimated using the geometric sequence approach, the Sauer method, the Palmans method, and the linear fit approach with the $TPR_{20,10}$ calculated using the TRS-398 protocol.

Specifically for the 6 MV X-ray beam in Table 9, the relative difference of the $TPR_{20,10}$ estimated using the geometric sequence approach was lower than the relative difference of the $TPR_{20,10}$ estimated using the Sauer method and Palmans method. This is because the equation for estimating $TPR_{20,10}$ used in the Sauer method is derived from the pattern of the $TPR_{20,10}$ at different field sizes in the BJR Sup. 25. As a result, the estimation of $TPR_{20,10}$ is closer to the $TPR_{20,10}$ reported in the BJR Sup. 25, which is 0.667 ± 0.003 [7].

The $TPR_{20,10}$ estimated using the Palmans method was also close to the $TPR_{20,10}$ reported in the

BJR Sup. 25, similar to the $TPR_{20,10}$ estimated using the Sauer method. This is because the equation for estimating $TPR_{20,10}$ used in the Palmans method is a modification of the Sauer equation. The constants A_1, A_2, b_1, b_2, t, and the exponential term in the Sauer method were simplified into only two constants, d_1 and d_2, by Palmans [6]. Furthermore, each variant of a LINAC has different specifications, so the baseline data of $TPR_{20,10}$ also differs for each variant [22]. The $TPR_{20,10}$ for the 6 MV X-ray beam of the LINAC used in this study was slightly different from the $TPR_{20,10}$ for the 6 MV X-ray beam reported in the BJR Sup. 25 [9].

Specifically for the 6 MV X-ray beam in Table 9, the relative difference of the $TPR_{20,10}$ estimated using the geometric sequence approach was greater than the relative difference of the $TPR_{20,10}$ estimated using the Sauer method, the Palmans method, and the linear fit approach. The lack of accuracy of the geometric sequence method when used to estimate the $TPR_{20,10}$ for the 10 MV X-ray beam can be inferred from the Durbin-Watson test results [16].

The Durbin-Watson test showed that no errors occured due to autocorrelation in the $TPR_{20,10}$ (s) for the 6 MV X-ray beam. However, the Durbin-Watson test showed that errors occured due to autocorrelation in the $TPR_{20,10}$ (s) for the 10 MV X-ray beam. As a consequence, in estimating the $TPR_{20,10}$ for the 10 MV X-ray beam, the geometric sequence and the linear fit approaches were less accurate than the Sauer method and the Palmans method [16]. Errors due to autocorrelation affected the accuracy of the linear regression equation and the ratio of the geometric sequence.

The Sauer method and the Palmans method were not affected by errors due to the autocorrelation. This is because the equations used in both the Sauer method and the Palmans method were derived from the $TPR_{20,10}$ (s) reported in the BJR Sup. 25, and were not derived from the $TPR_{20,10}$ (s) from the LINAC used in this study [6]. However, the equations used in the geometric sequence and linear fit approaches were not derived from the $TPR_{20,10}$ (s) reported in the BJR Sup. 25, instead they were derived from the $TPR_{20,10}$ (s) from the LINAC used in this study. However, all relative differences in Table 7 did not exceed ±1% from the baseline data of the $TPR_{20,10}$, which is desirable in this context [2].

CONCLUSION

The $TPR_{20,10}$ for the 6 MV and 10 MV X-ray beams estimated using the geometric sequence approach were 0.683 ± 0.004 and 0.742 ± 0.005, respectively. The geometric sequence approach has a level of precision equivalent to the TRS-398 protocol, the Sauer method, the Palmans method, and the linear fit approach. The $TPR_{20,10}$ for the 6 MV and 10 MV X-ray beams estimated using the geometric sequence approach did not show a significant difference compared with those $TPR_{20,10}$ calculated using the TRS-398 protocol and the linear fit approach. However, the $TPR_{20,10}$ for the 6 MV and 10 MV X-ray beams estimated using the geometric sequence approach showed a significant difference compared with those $TPR_{20,10}$ estimated using the Sauer method and the Palmans method.

ACKNOWLEDGMENT

The authors would like to thank Lavalette Hospital for providing the opportunity to conduct this study.

AUTHOR CONTRIBUTION

F.A. Rizaldi, S. Herwiningsih, and C.S. Widodo designed the study, calculated the $TPR_{20,10}$ using the geometric sequence approach, the Sauer method, the Palmans method, and the linear fit approach, and the TRS-398 protocol. They analyzed the data, performed statistical tests, and wrote the manuscript. F.K. Hentihu and A.K. Anto operated the LINAC, measure the PDD, D_{20cm}, D_{10cm}, and reviewed the manuscript.

REFERENCES

1. M. Aguilar, P. C. Qian, M. Boeck *et al*., Can. J. Cardiol. **37** (2021) 1818.
2. D. A. Roberts, C. Sandin, P. T. Vesanen *et al*., Med. Phys. **48** (2021) e67.
3. X.-J. Li, Y.-C. Ye, Y.-S. Zhang *et al*., PLoS One **17** (2022) 1.
4. International Atomic Energy Agency (IAEA), Absorbed Dose Determination in External Beam Radioteraphy, Technical Report Series 398, IAEA, Vienna, 2000.
5. A.M. Alssnusi, Y. A. Abdulla, N. A. Hussein *et al*., Atom Indones. **51** (2025) 243.
6. H. Palmans, Med. Phys. **39** (2012) 5513.
7. O. A. Sauer, Med. Phys. **36** (2009) 4168.
8. International Atomic Energy Agency (IAEA) Dosimetry for Small Static Fields Used in External Beam Radiotherapy, Technical Reports Series No. 483, IAEA, Vienna, 2017.

9. K. R. Mani, M. A. Bhuiyan, M.I. Hossain *et al*., Nucl. Sci. Appl. **26** (2017) 17.
10. F. E. M. Elbashir, W. Ksouri, F. Habbani *et al*., Appl. Sci. **12** (2022) 3857.
11. A. Z. Ibitoye, M. B. Adedokun, and I. K. Ogungbemi, Nig. J. Pure & Appl. Sci. **36** (2023) 4679.
12. P. H. Lam, P. T. Dung, and P. Q. Trung, Atom Indones. **50** (2024) 221.
13. A. Kercher, A. M. Bergman, and R. Zazkis, Can. J. Sci. Math. Techn. Educ. **23** (2023) 48.
14. V. Oxman, Int. J. Math. Educ. Sci. Technol. **57** (2024) 591.
15. M. M. Al-Kassab and A. H. Majeed, Adv. Appl. Stat. **81** (2022) 13.
16. S. L. Turner, A. B. Forbes, A. Karahalios *et al*., BMC Med. Res. Methodol. **21** (2021) 1.
17. D. Alesini, *Linear Particle Accelerators* (*LINAC)*, in: Proceedings of The CERN-Accelerator-School Course, CERN, Frascati (2021) 479.
18. A. Dróżdż, M. Waluś, M. Zieliński *et al*., Rep. Pract. Oncol. Radiother. **26** (2021) 1029.
19. S. Myers and H. Schopper, Particle Physics Reference Library, Volume 3: Accelerators and Colliders, Springer, Cham, 2020.
20. D. Lakens, Collabra Psychol. **8** (2022) 1.
21. G. Di Leo and F. Sardanelli, Eur. Radiol. Exp. **4** (2020) 1.
22. J. Tikkanen, K. Zink, M. Pimpinella *et al*., Phys. Med. Biol. **65** (2020) 1